Paper No.
2668

NACE INTERNATIONAL CORROSION 2013 CONFERENCE & EXPO

Modeling Nuclear Containment Liner Steel Liner Corrosion

Alberto Sagüés
University of South Florida
4202 East Fowler Ave
Tampa, Florida 33784
USA

Joseph Fernandez
University of South Florida
4202 East Fowler Ave
Tampa, Florida 33784
USA

ABSTRACT

Corrosion of containment liners has been observed on the outside surface that is in contact with the concrete containment building. Corrosion initiated on the outer surface of the liner, or the surface that is in contact with the concrete containment building wall, has been associated with foreign material left embedded in the concrete. Macrocell-accelerated localized corrosion appears to be the corrosion mechanism for outer diameter corrosion (OD-corrosion) of steel containment liners. Once initiated, localized corrosion can continue to propagate over a period of many years because the thick sections of concrete have sufficient water content and the ionic conductivity necessary to support the electrochemical corrosion reactions. The model presented depicts the electrochemical current density (and therefore corrosion rate) estimated due to the steel liner and rebar interaction with the foreign material at the point the foreign material is in contact with the liner. The model can be used to determine the probability of containment liner failure due to corrosion for the possible situation of a foreign material at the liner/concrete interface creating the macrocell as discussed above.

Key words: Macrocell Corrosion, Steel Containment Liner, Computer Modeling, Non-Destructive Evaluation

INTRODUCTION

Several instances of corrosion of steel containment liners has been observed on the outside surface that is in contact with the concrete containment enclosure.[1] It has been concluded that corrosion is initiated by the presence of an embedded foreign material in contact with the steel, such as wood pieces left in place at the time of casting. That material alters the local chemistry, for example by lowering the pH, thus preventing passivation of the steel liner at the concrete/liner interface and

creating a situation not unlike that of crevice corrosion.[2] A macrocell is formed whereby the local anodic area, where active corrosion is occurring, is coupled to a large cathodic surface that consists of passive sections of the liner immediately adjacent to the anodic area as well as multiple layers of rebar. This type of situation in concrete has received frequent attention in the literature.[3,4]

The current state of Non-Destructive Evaluation (NDE) technology may not be capable of effectively detecting OD-corrosion when considering the size of the containment structures and the area of the liner surface. While ultrasonic inspections can detect corrosion at point locations, it is challenging to apply currently available technology over large areas. Mitigation methods, mainly cathodic protection, may not be practical for preventing liner corrosion. A detailed understanding of the factors responsible for the extent of corrosion and its localization is desirable for forecasting possible future incidence of the problem, interpret survey results to identifying the location of corrosion spots in the liner, and establish mitigation procedures. An initial simplified model of the macrocell configuration was previously presented by one of the authors.[2] In this paper a physical model of the corroding system introducing additional details is presented to aid in improving that understanding and as a means of assessing the merits of the earlier simplified treatment.

DESCRIPTION OF THE MACROCELL CORROSION SCENARIO [(1)]

The scenario modeled here is similar to the one presented earlier, assuming that a piece of foreign material is embedded in the containment building concrete and in contact with the steel liner. The region of contact is assumed to be corroding in the active condition. There the anodic process is treated as being divalent iron dissolution:

$$Fe \rightarrow Fe^{2+} + 2e^{-} \quad (1)$$

with a rate following Butler-Volmer kinetics:[3,5]

$$i_a = i_{oa} \exp^{(Es-E_{oa})/\beta a} \quad (2)$$

where i_a is the rate of the anodic reaction (as a current density), i_{oa} is a nominal exchange current density, Es is the local potential, E_{oa} indicates the nominal equilibrium potential for the Fe oxidation reaction, and βa is the Tafel slope for the anodic reaction. No concentration limitation is assumed to occur. Es is assumed to be sufficiently above E_{oa} to ignore the reverse, Fe-reduction reaction. The cathodic process is assumed to be oxygen reduction, simplified as:

$$O_2 + 2H_2O + 4e^{-} \rightarrow 4OH^{-} \quad (3)$$

and to take place both at the corroding spot and in any surrounding passive steel regions. The local rate of oxygen reduction (i_c) is also taken to follow Butler-Volmer kinetics adapted as:

$$i_c = - i_{oc} (c_S/c_{EXT}) \exp^{(E_{oc}-Es)/\beta c} \quad (4)$$

[(1)] Parts of this section reproduce material presented by one of the authors (A.S) in a previous report.[2]

where i_{oc}, E_{oc} and β_c are the corresponding nominal kinetic parameters for the cathodic reaction, and c_S and c_{EXT} are the concentration of oxygen in the concrete at the steel concrete interface and at the atmospherically exposed concrete surface respectively. Hence the cathodic reaction rate is subject to transport limitations reflecting the extent to which oxygen was present initially in the medium and how efficiently it can be replenished by transport from the outside. The overall treatment follows the approximations and assumptions stated in previous work that can be consulted for further detail. [3]

For simplicity, the foreign material footprint is assumed to be circular and in a middle of a portion of the liner that is also circular with a radius in the order of half of the distance to other similar spots. Assuming that the spots are widely separated (e.g. many meters apart) and considering that the liner is comparatively thin (e.g. 1.2 m thick), the situation was abstracted as a cylindrical symmetry 2-dimensional equivalent as shown in the sketch in Figure 1. There the centrally active, circular net anodic spot of radius r is coupled to a cathodic outer ring (outer radius R) representing the surrounding passive liner material. In this abstraction the additional cathodic steel reinforcement surface embedded in the concrete is ignored. This latter simplification can be relieved in future analyses but as it will be shown, much of the macrocell action effect can be explained with the present abstraction without need for invoking the added reinforcement surface. The concrete is treated as a body with uniform electric resistivity ρ, and also as a medium where oxygen flow proceeds by diffusional transport with uniform diffusivity D. Hence and analogous to previous treatments in similar systems, [2] the electric potential E and oxygen concentration c within the concrete satisfy

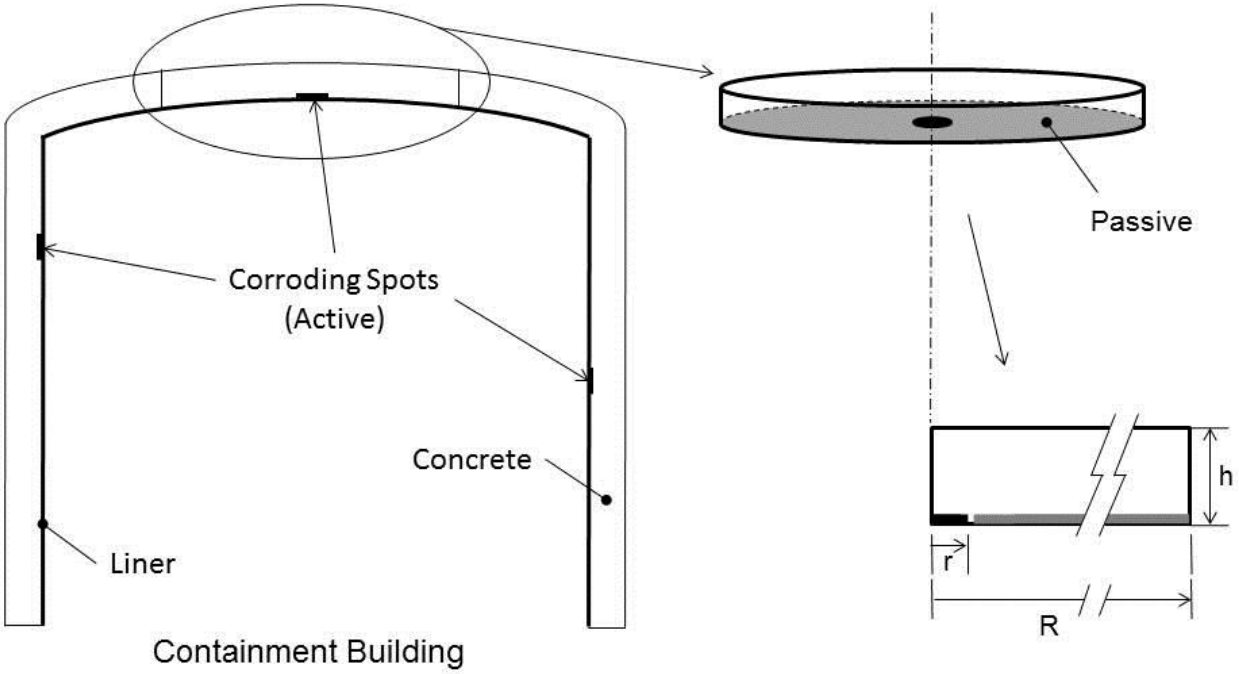

Figure 1: Diagram of Containment Section Represented by Modeled Cylinder

$$\nabla^2 E = 0 \quad (5)$$

$$\nabla^2 c = 0 \quad (6)$$

The outermost edge of the concrete domain is treated as a symmetry boundary with respect to similar neighboring regions so neither electric nor mass flow exists there. Hence in that boundary the gradient in the radial direction for both E and c are set to zero.

In the upper concrete boundary in contact with air the pore water in the concrete is assumed to be in equilibrium with atmospheric oxygen so there $c = c_{EXT}$. At that boundary the concrete terminates so no current flow exists and therefore the gradient of E is set to zero. The left boundary of the concrete domain is the rotational axis of symmetry and all radial gradients there are zero as well.

At the lower boundary of the domain the ruling boundary conditions are given by equations (2) and (4) for the corroding spot as well as only (4) for the passive region, and linking those interfacial currents to the macrocell current flow in the concrete by:

$$N^*\rho^{-1} \nabla E = i \quad (7)$$

where i = ia + ic for the corroding spot and i = ic for the passive region, and N represents a normal vector to the interface with appropriate orientation for correct sign.

Moreover, the diffusional flow of oxygen to the steel surface is linked to the cathodic current by the Faradaic relationship:

$$N^*D \nabla c = i_c/nF \quad (8)$$

Replicating the approach used in the earlier simplified calculations,[2] conditions bracketing by extremes a plausible range were adopted. Table 1 lists the parameter values used. The model was implemented by considering corroding spots of sizes ranging from small (r=1) to large (r=10 cm), and for a range of concrete resistivities ranging from very low (10 ohm-cm), representative of wet and highly permeable concrete, to very large (1000 ohm-cm) which would represent either very dry permeable concrete, or extremely low permeability concrete in a moist condition. In most cases D was assumed to be 1e-8 m^2/s, a value representative of mid conditions for atmospherically exposed concrete. One instance of much lower value, D=1e-10 was used to examine the behavior that might take place when the pore network is occluded by nearly water-saturated conditions. The selection of values of D is described can be found described in more detail in a previous publication. [3] The values of the kinetic polarization parameters are subject to uncertainty, so values approximating those used in a prior simulation of comparable systems [3] were tentatively adopted.

The modeling was implemented in a COMSOL Multiphysics 4.2a[(2)] platform. From this program, the Electric Currents part of the AC/DC Module was used along with the Transport of Diluted Species part of the Chemical Species Transport Module.

[(2)] Trade Name

Table 1
Simulation Parameters

Description	Symbol	Values and Units
Radius of Concrete Domain	R	5 m
Radius of Foreign Object	r	0.01, 0.03, 0.1 m
Concrete Thickness	h	1.2 m
Nominal Equilibrium Potential, Anodic Reaction	E_{oa}	-0.78 V (SCE)*
Nominal Equilibrium Potential, Cathodic Reaction	E_{oc}	0.16 V (SCE)
Tafel Slope, Anodic Reaction	βa	0.06 V
Tafel Slope, Cathodic Reaction	βc	0.16 V
Concentration of Oxygen at External Concrete Surface	c_{EXT}	0.25 mol/m^3
Nominal Exchange Current Density, Anodic Reaction	i_{oa}	3e-4 A/m^2
Nominal Exchange Current Density, Cathodic Reaction	i_{oc}	1e-5 A/m^2
Concrete Resistivity	ρ	10, 100, 1e3 ohm-m
Concrete Oxygen Diffusivity	D	1e-8, 1e-10 m^2/s

*Steel potentials are given as if measured in the conventional manner (E_{steel} - $E_{reference\ electrode}$). Computations were actually conducted with potentials in concrete referred to that of steel.

RESULTS AND DISCUSSION

The primary model output was the steady state value of the electric potential and oxygen concentration at each point in the concrete domain. Application of the ruling equations then yields the current density of the cathodic and anodic reactions at the steel surface and hence the corrosion rate distribution.

Figure 2 illustrates in the cylindrical cross section the potential distribution and corresponding current density lines for a case with r=0.1 m, ρ=100 ohm-m and D=1e-8 m^2/s, hereinafter named Case A. Figure 3 (Top) shows the corresponding oxygen distribution pattern. Figure 2 shows clearly that for this case much of the macrocell current originating at the anodic spot is distributed broadly over the passive region. Figure 3 (Top) shows that oxygen starvation in Case A is limited mostly around the corroding spot and that it does not affect greatly the rest of the passive region.

Figure 4 shows for Case A the distribution of potential and of macrocell current density within a 0.5 m radius around the center. The overall trends are as expected, with net anodic and cathodic behavior in the corroding spot and passive region respectively. Also as expected, the anodic current density peaks around the edge of the corroding spot and both the anodic and cathodic current densities decrease away from that edge.[3]

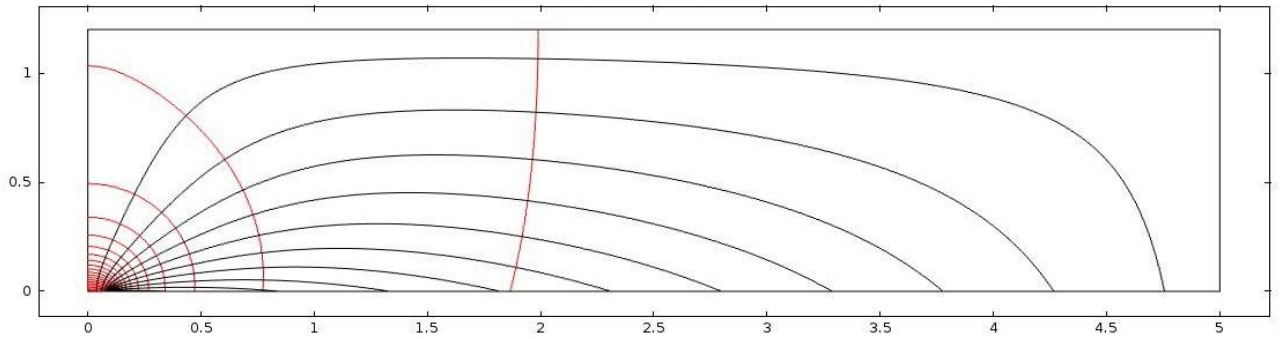

Figure 2: Potential distribution and current lines in the concrete domain cylindrical cross section (Case A: r=0.1 m, r=100 ohm-m and D=1e-8 m2/s). Dimensions in m. Rightmost isopotential contour: 0.0618 V; step: 36.2 mV.

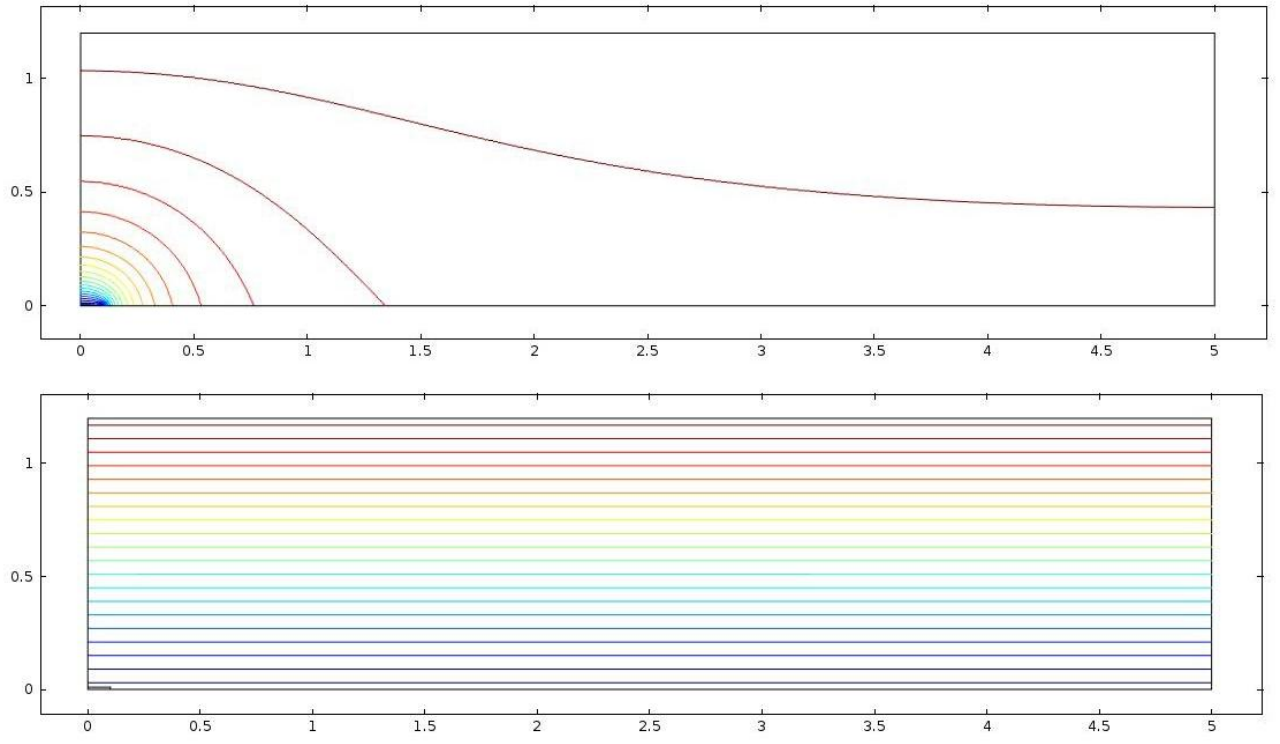

Figure 3: Oxygen concentration distribution for Case A (Top); same parameters as in Case A except D=1e-10 m^2/s (Bottom). Dimensions in m. Highest isoconcentration contour is 0.2438 mol/m^3; step: 12.5 mmol/m^3

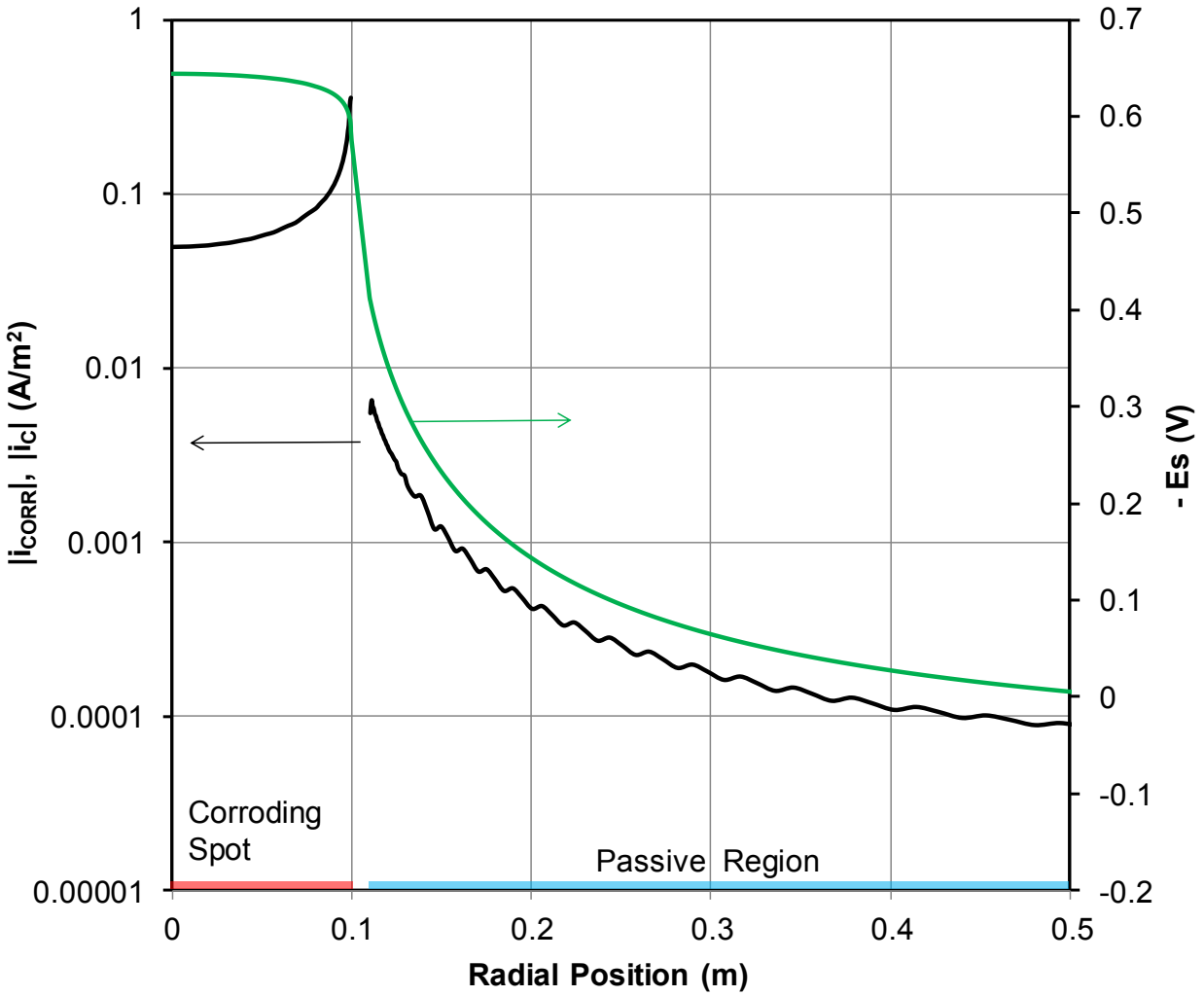

Figure 4: Steel Potential and Absolute Value of the Macrocell Current density at the concrete facing the steel surface $|i| = |i_a + i_c|$ near the Corroding Spot for Case A. Fine structure around the main decreasing trend with radius in the passive region is an artifact from FEM meshing and the small magnitude of i_c there.

The cathodic current density however is one or more orders of magnitude smaller than that of the anodic spot, consistent with the spread of the cathodic current over a vastly larger area, as indicated in Figure 2. Integration of the anodic and cathodic macrocell currents over their respective areas yielded absolute values of 2.886e-3 and 2.880e-3 A, thus differing from each other by <0.3%, attesting to internal consistency of the calculations. Comparably good current balance levels were obtained for the others simulated conditions. Integration of the anodic current density by itself in the corroding spot yielded nearly the same value as that of the macrocell current, indicating that the extent of the cathodic reaction was small there due to local oxygen starvation. This is consistent with the oxygen distribution pattern shown in Figure 3 (Top). Calculation of the average corrosion current density on the corroding spot yielded a value of i_{corrav} = 1.01e-1 A/m^2. By Faradaic conversion (for Fe+2 ion production 1 μA/cm^2 → ~11.6 μm/y)[7] , the corresponding average corrosion rate in the central disk is 117 μm/y. A summary of similar evaluations for all the other conditions modeled is presented in Figure 5.

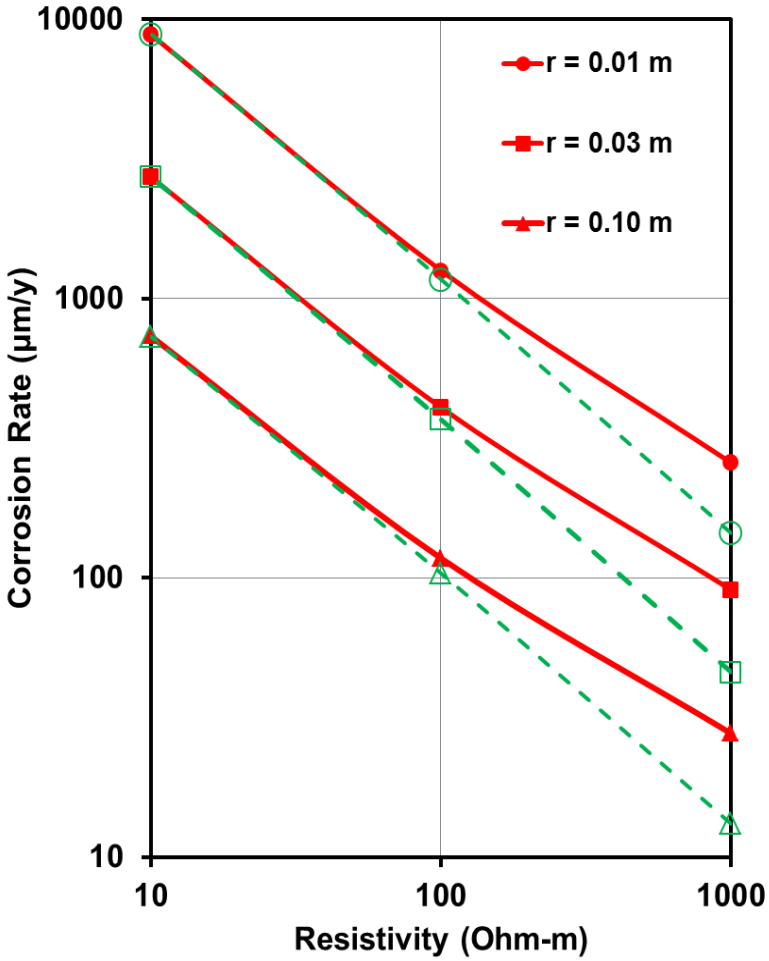

Figure 5: Red symbols: projection of average corrosion rate in the corroding spot as function spot radius and concrete resistivity. Green symbols: Comparison with projection from previous work[2] after adjusting for macrocell driving potential (see text).

Examination of the potential distribution showed that further away from the corroding spot and over much of the passive region, the cathodic reaction was polarized ~0.1 V from its nominal equilibrium potential, and that on the corroding spot the corresponding polarization of the anodic reaction was of

about the same order. For Case A the overall macrocell driving potential E_m, defined as the area-averaged potential for the passive region minus that of the corroding spot, was E_m = 0.703 V. The values of Em for the other conditions sampled are listed in Table 2

Table 2
Macrocell Driving Potential Em (V)

ρ (ohm-m)	Corroding Spot Radius r (m)		
	0.1	0.03	0.01
1000	8.91E-01	9.34E-01	9.79E-01
100	7.03E-01	7.49E-01	7.93E-01
10	4.94E-01	5.55E-01	6.00E-01

The relative corrosion rate trends shown in Figure 5 largely resemble those obtained with the earlier simplified modeling approach.[2] In that treatment corrosion control was assumed to be entirely ohmic, the anodic and cathodic regions were purely so, and the macrocell driving potential was considered to be a constant. Consequently, the projected corrosion rate was simply inversely proportional to the increase in assumed concrete resistivity. In the present model the projected corrosion rate of the active spot also decreases with increasing resistivity, but the trend slopes in the log-log representation in Figure 5 are less pronounced than -1 (which would have indicated exact inverse proportionality), especially for the larger concrete resistivity range. That behavior takes place because the present model additionally captures changes in the polarization of the reactions at both the anodic and cathodic regions. Consequently, as the ohmic resistance becomes greater and current decreases, the extent of polarization of each of the reactions becomes less, so E_m increases, sometimes considerably as shown in Table 2. As a result, the effect of the increasing resistance is mitigated to some extent so the resulting trend slope is more moderate. Furthermore, the present model also differentiates between the macrocell and the corrosion current. That difference becomes greater at the higher resistivity range, where the coupling between the passive region and the corroding spot is less efficient and hence local cell action is stronger. It is noted that the relative trend in changing corrosion rate with varying spot size is nearly exactly inversely proportional in both the earlier and the present models. This observation is consistent with the results in Table 2, which show that for a given concrete resistivity value E_m is not greatly sensitive to the value of r. Clearly there is a mutual cancelation of effects in this case, but an explanation as to why necessitates further study.

The present model, as the earlier treatment, projects substantial corrosion rates for the affected spots. For a mid-conditions case such as r = 0.03 m and r = 100 ohm-m, the projected rate is ~0.4 mm/y which would imply penetration of a 1-cm thick liner after some 30 years of service. Such duration is in the order of the service times (several decades) that have resulted in observed liner penetration.[1,2] The precise value of the projected corrosion rates is however about 3 times greater in the present model than in the earlier approach. The main reason for that discrepancy is the choice of present model parameters as listed in Table 1. As indicated earlier, the nominal equilibrium potentials and exchange current densities listed there are tentative values in lieu of actual data for these systems. The resulting values of E_m, listed in Table 2, range from 0.49 V to as much as 0.98 V, which are almost 2 to 4 times greater than the flat value of 0.25 V conservatively adopted in the earlier model implementation.[2] Continuation work will explore the use of more representative polarization parameters. There, the geometry of the system was abstracted as that of an anodic disk placed on an isolating plane in contact with an electrolyte which has a remotely placed cathode of infinite dimensions. Such configuration results in a current constriction effective resistance,[9] R_c given by

$$R_c = \rho / 4r \qquad (9)$$

Hence, the macrocell current results in an average current density at the anode given by[2]

$$i_{corr} = E_m / \pi r \rho \quad (10)$$

so that the resulting corrosion current (simplified in that approach as being the same as the macrocell current) is directly proportional to the value of E_m.

To explore the extent to which that simple disk in semi-infinite domain treatment might approach the present model results, Equation (10) was applied using the values of E_m for each case listed in Table 2, and the resulting i_{corr} was then converted into a corrosion rate. The resulting adjusted values are plotted in Figure 5 (green symbols), showing remarkably good agreement with the direct model calculations in the lower resistivity range. Such agreement is consistent with the current distribution trends apparent in Figure 2 and detailed in Figure 4, that show that the cathodic current density on the passive region, even when very close to the anode, is quite small, thus providing a reasonable approximation of the anode behavior to that of an anode in an otherwise isolated plane. This observation suggests also that, at least for the $D=10^{-8}$ m^2/s cases explored here, the large cathodic surface provided by the rest of the liner alone can deliver substantial total current amounts with only modest polarization. Hence, the effect of the other reinforcement in the system that was not considered in the present model, while finite, may at least in some instances not result in a dramatic increase in the corrosion of the active spots.

As noted above, when the concrete resistivity is very high (1000 ohm-m cases) the simple earlier macrocell current model projections underestimated those of the more detail present model. Rough estimates of the limiting oxygen reduction current for those cases, using the diffusion equivalent of Equation (9), show that the difference between both model projections approximately matches the expected limiting oxygen reduction current for the given spot size and assumed diffusivity.

Initial findings for lower oxygen diffusivity cases are exemplified by that illustrated in Figure 3 (Bottom), and indicate as expected that the overall extent of corrosion is limited by the possible oxygen supply to the steel surface. In that situation the corrosion rate of the active spot equals almost entirely the macrocell current since the amount of local cell action there is comparatively very small given the relative large difference in areas. The projected corrosion rate in that case for r=10 cm is smaller (23 μm/y) than that for Case A (117 μm/y) but could still become important for smaller corroding spot sizes. Ongoing work is addressing those scenarios.

CONCLUSIONS

A proposed localized corrosion scenario, together with assumption of tentative but generally plausible kinetic parameters and concrete properties, were used to formulate a quantitative damage projection model for liner penetration incidents. The model was based on a 2-dimensional geometry with cylindrical geometry.

The model corrosion rate projections were consistent with the time frame of observed penetration events.

The model, incorporating polarization of the corrosion reactions in addition to ohmic limitation, yielded trends that were comparable to those obtained in an earlier approach where only macrocell-driven corrosion rates were assumed.

ACKNOWLEDGEMENTS

The authors thank the University of South Florida, as well as the Alfred P. Sloan Foundation for their material support of this study (*The opinions, findings, and conclusions expressed here are those of the author and not necessarily those of any supporting organizations*).

.

REFERENCES

1. D. S. Dunn, A. L. Pulvirenti, and M. A. Hiser, “Containment Liner Corrosion Operating Experience Summary”, Technical Letter Report, Nuclear Regulatory Commission, Office of Nuclear Regulatory Research, 2010.

2. J. P. Petti, D. Naus, A. A. Sagüés, R. E. Weyers, B. A. Erler, N. S. Berke “Nuclear Containment Steel Liner Corrosion Workshop: Final Summary and Recommendation Report,” SAND2010-8718, Albuquerque, New Mexico: Sandia National Laboratories, July 2011.

3. S. C. Kranc, A. A. Sagüés “Computation of Reinforcing Steel Corrosion Distribution in Concrete Marine Bridge Substructures,” Corrosion, Volume 50, Number 1, p. 50, January 1994.

4. A. A. Sagüés, M. A. Pech-Canul, and, A. K. M. Shahid Al-Mansur, “Corrosion Macrocell Behavior of Reinforcing Steel in Partially Submerged Concrete Columns”, Corrosion Science, Volume 45, p. 7, 2003.

5. D. D. MacDonald, “Transients Techniques in Electrochemistry”, Plenum Press, New York, 1977.

6. J. E. Winandy and R. M. Rowell, Chemistry of Wood Strength, Chapter 11, “Handbook of Wood Chemistry and Composites”, CRC Press Boca Raton, 2005.

7. D. A. Jones, “Principles and Prevention of Corrosion”, 2nd Edition, Prentice Hall, Upper Saddle River, 1996.

8. L. Bertolini, B. Elsener, P. Pedeferri, and R. Polder, “Corrosion of Steel in Concrete”, Wiley, Weinheim, 2004.

9. R. Oltra, M. Keddam, “Application of Impedance Technique to Localized Corrosion”, Corrosion Science, Volume 28, p. 1, 1988.